viruses

MDPI

Article

Isolation and Characterization of Bacteriophages Targeting *Escherichia coli* from Companion Animal UTIs: Resistance-Associated Macrolide Susceptibility and Fitness Costs

Mana Tohyama [1,2,†], Haruka Ohashi [2,†], Tomohiro Nakamura [2,3,4,5,†], Jumpei Fujiki [2,†], Kentaro Morikawa [2], Naomi Iwano [6], Masashi Ebisawa [6], Hiroki Inoue [2,6], Tomohito Iwasaki [7] and Hidetomo Iwano [2,4,*]

[1] Laboratory of Veterinary Hygiene, Graduate School of Infectious Diseases, Hokkaido University, Sapporo 060-0818, Japan; tohyama.mana.a1@elms.hokudai.ac.jp
[2] Laboratory of Veterinary Biochemistry, School of Veterinary Medicine, Rakuno Gakuen University, Ebetsu 069-8501, Japan; t-nakamura@azabu-u.ac.jp (T.N.); j-fujiki@rakuno.ac.jp (J.F.); hinoue@ndts.co.jp (H.I.)
[3] Department of Drug Development, National Institute of Infectious Diseases, Japan Institute for Health Security, Tokyo 162-8640, Japan
[4] Phage Therapy Institute, Comprehensive Research Organization, Waseda University, Tokyo 162-8480, Japan
[5] Laboratory of Small Animal Surgery, School of Veterinary Medicine, Azabu University, Sagamihara 252-5201, Japan
[6] NDTS Co., Ltd., Sapporo 004-0015, Japan; iwano@ndts.co.jp (N.I.); ebisawa@ndts.co.jp (M.E.)
[7] Department of Food Science and Human Wellness, College of Agriculture, Food and Environment Science, Rakuno Gakuen University, Ebetsu 069-8501, Japan; iwasaki@rakuno.ac.jp
* Correspondence: h-iwano@rakuno.ac.jp
† These authors contributed equally to this work.

Abstract

Urinary tract infections (UTIs) in companion animals are often associated with antibiotic-resistant *Escherichia coli*. We screened approximately 110 sewage samples against 35 clinical isolates, yielding 23 phages. Three phages, ΦF24, ΦH28-2, and ΦH27, were selected for detailed characterization against UTI-associated *E. coli* isolates. ΦF24 and ΦH28-2 showed activity against multiple isolates, and ΦH28-2 showed sustained suppression of EcudH growth over 24 h. Genome analysis classified ΦF24 and ΦH28-2 as *Tequatrovirus* and ΦH27 as *Felixounavirus*. Phage-resistant variants revealed mutations in the lipopolysaccharide (LPS) core biosynthesis genes (*waaO* and *waaT* in ΦH27-resistant derivatives and *waaC* in ΦH28-2-resistant derivatives), the ADP-heptose biosynthesis gene *hldE* in a ΦH28-2-resistant derivative, and the outer-membrane protein gene *ompA* in ΦF24-resistant derivatives. Knockout analysis suggested that ΦH28-2 infection requires a WaaC-dependent LPS inner-core structure containing heptose I. ΦH28-2-resistant derivatives also showed reduced culture growth in antibiotic-free medium. Furthermore, these strains exhibited increased susceptibility to erythromycin and clarithromycin, including at 2 μg mL^{-1}, a concentration at which the parental strain was less affected. Moreover, co-exposure to ΦH28-2 and clarithromycin further reduced growth at 12 h compared with phage treatment alone in a separate clinical isolate. These findings highlight the potential of ΦH28-2 as a therapeutic candidate and suggest an association between LPS inner-core alterations, reduced growth yield, and increased macrolide susceptibility.

Academic Editor: Mikael Skurnik

Received: 31 October 2026
Revised: 22 November 2026
Accepted: 23 November 2026
Published: 29 November 2026

Copyright: © 2026 by the authors. Licensee MDPI, Basel, Switzerland. This article is an open access article distributed under the terms and conditions of the Creative Commons Attribution (CC BY) license.

Keywords: bacteriophage; *Escherichia coli*; urinary tract infection; companion animals; lipopolysaccharide inner core; phage resistance; macrolide susceptibility; evolutionary trade-off; phage therapy

1. Introduction

Antimicrobial resistance (AMR) has become a serious global health problem, with substantial morbidity and mortality worldwide [1]. Among antimicrobial-resistant pathogens, *Escherichia coli* (*E. coli*) is one of the most clinically important species, contributing substantially to the global burden of bacterial infections [2]. Certain strains of *E. coli*, collectively referred to as extraintestinal pathogenic *E. coli* (ExPEC), are capable of causing infections outside the intestinal tract [3]. *E. coli* is the leading causative agent of urinary tract infections (UTIs), including community- and hospital-acquired infections [4,5]. Antimicrobial resistance among UTI-associated *E. coli* isolates further complicates treatment [6].

AMR is an issue of growing concern in the field of veterinary medicine. In companion animals, *E. coli* is one of the most frequent causes of bacterial UTIs [7]. The emergence of antimicrobial-resistant *E. coli* in these animals not only complicates treatment but also raises One Health concerns regarding the potential spread of resistant bacteria between animals and humans. Therefore, alternative strategies to control drug-resistant *E. coli* infections in companion animals are urgently needed.

Currently, antibiotics are the primary treatment for bacterial UTIs; however, acquired resistance can compromise their effectiveness, while intrinsic resistance limits the activity of certain antibiotic classes. Macrolides, such as erythromycin and clarithromycin, inhibit bacterial protein synthesis and exhibit activity against many Gram-positive bacteria and mycoplasmas. However, their activity against *E. coli* is generally limited by restricted outer-membrane penetration and active efflux [8,9]. Lipopolysaccharide (LPS) contains hydrophilic carbohydrate regions, including the core oligosaccharide and, in smooth strains, the O-antigen polysaccharide, and contributes to the outer-membrane permeability barrier against hydrophobic compounds [10]. Alterations in LPS carbohydrate structure, particularly truncation of the core oligosaccharide, can compromise this barrier and increase susceptibility to hydrophobic antibiotics, including macrolides.

Under these circumstances, phage therapy, which utilizes bacteriophages, has regained attention as a potential alternative or adjunct to conventional antibiotics. One of its main advantages is high host specificity, which enables targeted killing of susceptible bacteria and may limit effects on non-target microbiota. Furthermore, because phages have mechanisms of action distinct from those of antibiotics, they may retain activity against antibiotic-resistant bacteria. In addition, phage resistance can sometimes be associated with increased susceptibility to antibiotics, a phenomenon described in preclinical studies and reviews [11–13]. Phages with in vitro lytic activity against canine and feline uropathogenic *E. coli* have also been described [14]. However, the narrow host range of individual phages and the emergence of phage-resistant bacteria remain key challenges. Phage resistance can nevertheless be accompanied by trade-offs, including reduced bacterial growth or increased antibiotic susceptibility [15,16]. In uropathogenic *E. coli*, resistance associated with LPS biosynthesis mutations has been linked to reduced growth in urine and increased susceptibility to membrane-targeting antibiotics [17].

These findings support evaluating both phage activity and resistance-associated phenotypes in companion-animal isolates. In this study, we isolated and characterized three phages, ΦF24, ΦH28-2, and ΦH27, targeting UTI-associated *E. coli* isolated from

companion animals. We evaluated their host range, lytic activity, genomic features and genetic changes associated with phage resistance. Furthermore, we examined resistance-associated changes in bacterial growth and macrolide susceptibility and evaluated bacterial growth during combined exposure to ΦH28-2 and clarithromycin in vitro.

2. Materials and Methods

2.1. Bacterial Strains

The clinical *E. coli* isolates used in this study were obtained from companion animals with urinary tract infections. The ERIKA strain was provided by the Rakuno Gakuen University Animal Medical Center (Ebetsu, Japan), and the remaining clinical isolates were provided by VDT Corporation (Fujisawa, Japan). *E. coli* K-12 BW25113 and its isogenic Keio collection mutants JW3596 (Δ*waaC*) and JW3595 (Δ*waaF*) were obtained from the National BioResource Project (NBRP), National Institute of Genetics (Mishima, Japan) [18].

2.2. Transmission Electron Microscopy

Phage preparations for transmission electron microscopy were purified by ultracentrifugation as previously described [19]. Purified phages in SM buffer (50 mM Tris-HCl, pH 7.5; 100 mM NaCl; 8 mM $MgSO_4$; 0.01% gelatin) were applied to collodion support films and negatively stained with 2% uranyl acetate. Phage morphology was examined using an H-800 transmission electron microscope (Hitachi, Tokyo, Japan) operated at an accelerating voltage of 75 kV [19,20].

2.3. Isolation of Phages

Phages were isolated from sewage samples. The samples were centrifuged at 8000× *g* for 10 min at 4 °C, and the supernatants were filtered through a 0.45 μm pore-size membrane filter (ADVANTEC, Tokyo, Japan) and stored at 4 °C.

For phage screening, *E. coli* host cells were mixed with 100 μL of the filtered sewage sample. The mixture was added to 3 mL of LB agar containing 0.5% agar and overlaid onto LB agar plates. Plates were incubated overnight at 37 °C using the double-layer agar (DLA) method. Phage-positive samples were identified by the formation of plaques on the bacterial lawn.

For plaque purification, phage-positive samples were serially diluted in SM buffer and plated with the host strain using the DLA method. The next day, a single plaque was picked with a pipette tip, transferred into 1 mL of LB broth, and incubated at 37 °C for 2 h. After incubation, the suspension was centrifuged at 10,000× *g* for 5 min, and the supernatant was collected. This plaque purification procedure was repeated twice, and the final supernatants were designated as purified phage stocks.

2.4. Purification and Titer Measurement of Phages

Each purified phage sample was propagated with the host strain using the DLA method until confluent lysis was observed. The next day, 3 mL of SM buffer was added to each plate, and the plates were incubated at 37 °C for 30 min. The liquid was then collected in tubes and centrifuged at 8000× *g* for 10 min at 4 °C, and the supernatant was filtered through a 0.45 μm pore-size membrane filter to obtain the plate lysates.

Phages were purified from the plate lysates using the Phage on Tap (PoT) protocol [21]. This protocol involves centrifugation and filtration through a 0.45 μm pore-size membrane filter, followed by concentration and purification using a 100 kDa molecular weight cut-off ultrafiltration device Amicon® Ultra-15 centrifugal filter device (Merck

Millipore Ltd., Darmstadt, Germany) and buffer exchange into SM Buffer. The final product was designated as the PoT product and was stored at 4 °C.

Phage titers were determined by plaque assays using the DLA method. The plate lysate or PoT product of each phage was serially diluted in SM Buffer and plated with the host bacterium using the DLA method. The next day, plaques on the plates were counted. The titer of the phage sample was calculated and expressed as plaque-forming units per milliliter (PFU/mL) based on the number of plaques, the dilution factor, and the volume used in the assay.

2.5. Spot Assay

Phage susceptibility was assessed by spot assays. In this assay, 100 µL of a culture of the test strain was added to 3 mL of LB top agar, and the mixture was overlaid onto LB agar plates. Tenfold serial dilutions of each purified phage preparation (PoT product), ranging from 10^8 to 10^1 PFU/mL, were prepared in SM buffer. Then, 2 µL of each dilution was spotted onto the bacterial lawn. Plates were incubated overnight at 37 °C, and lysis at the spotting sites was recorded.

2.6. Determination of Efficiency of Plating (EOP)

The efficiency of plating (EOP) was determined using a spot assay. EcudH was used as the reference strain for all three phages. The propagation hosts were EcudF for ΦF24 and EcudH for ΦH27 and ΦH28-2. Phage suspensions were serially diluted tenfold (10^0–10^{-7}), and 2 µL of each dilution was spotted onto bacterial lawns of the reference and test strains. Only clearly distinguishable plaques were counted; diffuse lysis zones were not included in the counts. Phage titers were calculated as PFU/mL. EOP was calculated as the ratio of the phage titer on each test strain to that on the reference strain, EcudH. Each measurement was performed in triplicate, and the mean EOP was calculated.

2.7. Time-Course Analysis of Phage Lytic Activity Using a Plate Reader

Overnight cultures of bacterial strains were diluted 1:100 in fresh LB broth and incubated at 37 °C until the optical density at 600 nm (OD_{600}) reached approximately 0.4. Subsequently, 200 µL of the bacterial culture was dispensed into each well of a 96-well plate, and 20 µL of phage suspension (1×10^7 PFU/mL) was added to each well. Plates were incubated at 37 °C with shaking, and bacterial growth was monitored by measuring OD_{600} every 15 min for 24 h using a microplate reader (Sunrise Rainbow Thermo RC, Tecan Japan, Kanagawa, Japan).

2.8. Growth Kinetics of Clinical Isolates and Phage-Resistant Strains

Cultures of clinical *E. coli* isolates and phage-resistant strains were adjusted to an OD_{600} of approximately 0.4 and dispensed into 96-well microtiter plates. The plates were placed in a plate reader, and bacterial growth in LB broth was monitored by measuring OD_{600} every 15 min during incubation at 37 °C with shaking for 24 h. Each condition was tested in triplicate.

2.9. Isolation of Phage-Resistant Strains

Although ΦF24 was originally isolated using EcudF, all phage-resistant derivatives analyzed in this study were obtained from EcudH following exposure to ΦF24, ΦH27, or ΦH28-2. A clinical *E. coli* isolate was grown overnight in LB broth at 37 °C with shaking at 180 rpm. An aliquot of 40 µL of the overnight culture was added to 4 mL of fresh LB broth and incubated at 37 °C while shaking for 2 h. Then, 40 µL of phage solution (1.0×10^8 PFU/mL) was added, and the culture was further incubated at 37 °C with shaking for 48 h.

After incubation, the bacterial cells were washed four times with 4 mL of phosphate-buffered saline (PBS) at 4 °C. The bacterial suspension was streaked onto LB agar plates and incubated overnight at 37 °C. Single colonies were picked and individually inoculated into 3 mL of LB broth, followed by overnight incubation at 37 °C with shaking.

Phage resistance of the cloned isolates was evaluated by spot assays. Isolates that showed no lysis at the spotting sites were designated as phage-resistant strains. Clonal phage-resistant strains were stored at −80 °C in LB broth supplemented with 50% glycerol.

2.10. Whole-Genome Sequencing and Assembly

Genomic DNA was extracted from purified preparations of the three bacteriophages (ΦF24, ΦH28-2, and ΦH27) using the Phage DNA Isolation Kit (Norgen Biotek Corp., Thorold, ON, Canada). Genomic DNA was extracted from 35 clinical *E. coli* isolates using the NucleoBond® HMW DNA kit (MACHEREY-NAGEL, Düren, Germany), according to the manufacturer's instructions. For ΦF24, ΦH28-2, and the clinical *E. coli* isolates, sequencing libraries were prepared using the MGIEasy FS DNA Library Prep Set (MGI, Shenzhen, China) and the MGISP960 automated sample preparation system (MGI, Shenzhen, China). Sequencing was performed on a DNBSEQ-G400 platform (MGI, Shenzhen, China), generating 150 bp paired-end reads. For ΦH27, a sequencing library was prepared using the TruSeq Library Prep Kit (Illumina, San Diego, CA, USA), followed by 150 bp paired-end sequencing on an Illumina NovaSeq X platform (Illumina, San Diego, CA, USA). Raw sequencing reads were processed using Trimmomatic v0.39 [22] to remove low-quality bases, short fragments (<80 bp), and adapter sequences. De novo genome assembly was performed using Shovill v1.1.0 (https://github.com/tseemann/shovill, accessed on 25 November 2026) for ΦF24, ΦH28-2, and the clinical *E. coli* isolates, whereas Unicycler v0.5.1 [23] was used for ΦH27. For determination of the complete genome sequence of *E. coli* strain EcudH, additional short- and long-read sequencing was performed. For short-read sequencing, libraries were prepared using the MGIEasy FS DNA Library Prep Set (MGI, Shenzhen, China), and sequencing was performed on a DNBSEQ-G400 platform (MGI, Shenzhen, China), generating 200 bp paired-end reads. For long-read sequencing, libraries were prepared using the Ligation Sequencing Kit (Oxford Nanopore Technologies plc, Oxford, United Kingdom) and sequenced on a GridION platform (Oxford Nanopore Technologies plc, Oxford, United Kingdom) with an R9.4.1 flow cell. Base calling and barcode demultiplexing were performed using Guppy v6.1.5. Adapter sequences were removed from short reads using Cutadapt v4.0 [24], and approximately 3.5 million read pairs were subsampled using SeqKit v0.13.2 [25]. Low-quality bases were trimmed using Sickle v1.33 (https://github.com/najoshi/sickle, accessed on 25 November 2026), and read pairs were discarded if either read was shorter than 127 bp. For long reads, adapter sequences were removed using Porechop v0.2.3 [26], and reads of 1000 bp or shorter were excluded using Filtlong v0.2.0 (https://github.com/rrwick/Filtlong, accessed on 25 November 2026). The processed short and long reads were subjected to hybrid assembly using Unicycler v0.4.7 [23] with default settings. Assembly graphs were inspected using Bandage v0.8.1 [27], and genome completeness was evaluated using CheckM v1.1.2 [28]. The assembled phage genome sequences have been assigned DDBJ accession numbers LC969012 (ΦF24), LC969014 (ΦH28-2), and LC969013 (ΦH27). The complete EcudH genome has been assigned accession numbers AP054613 (chromosome), AP054614 (plasmid 1), and AP054615 (plasmid 2) under BioProject PRJDB45974 and BioSample SAMD02121473.

2.11. Phage Genome Annotation and Comparative Genomic Analysis

Coding sequences and putative gene functions in the assembled phage genomes were annotated using Pharokka v1.8.1 [29] and Phold v1.1.0 [30]. Circular representations

of the annotated genomes were generated using Phold v1.1.0. Comparative genomic analyses of ΦF24 and ΦH28-2 were performed using LoVis4u v0.1.6 [31] and clinker v0.0.28 [32] to assess genome organization and sequence conservation.

2.12. Phylogenetic Analysis of Bacteriophages

Whole-genome phylogenetic analyses were performed using VICTOR [33]. Reference phage genomes belonging to the genera *Tequatrovirus* and *Felixounavirus* were selected from the International Committee on Taxonomy of Viruses (ICTV) Virus Metadata Resource (VMR_MSL39_v1.4.2).

2.13. Genomic Characterization and Phylogenetic Analysis of Clinical E. coli Isolates

The assembled genomes of the 35 clinical E. coli isolates were annotated using Prokka v1.14.6 [34]. Multilocus sequence typing (MLST) was performed using mlst v2.25.0 [35] to determine the sequence types (STs) of individual isolates. In silico serotype prediction was performed using ECTyper v2.0.0 [36] to identify the O- and H-antigen types based on the assembled genome sequences. Core-genome phylogenetic analysis was conducted using Panaroo v1.5.2 [37] and IQ-TREE v3.0.1 [38]. The GFF files generated by Prokka were used as input for Panaroo, which was run in strict cleaning mode with the removal of invalid genes. Core-gene sequences were aligned using MAFFT through the Panaroo core-alignment workflow. A maximum-likelihood phylogenetic tree was constructed from the concatenated core-gene alignment using IQ-TREE. The best-fitting nucleotide substitution model was selected using ModelFinder, and branch support was evaluated with 1000 ultrafast bootstrap replicates. The resulting phylogenetic tree was visualized using Interactive Tree Of Life (iTOL) v7 [39].

2.14. Mutation Analysis of Phage-Resistant Strains

Phage-resistant strains were cultured overnight in LB broth, and genomic DNA was extracted and purified using the NucleoBond HMW DNA kit (MACHEREY-NAGEL, Düren, Germany). DNA sequencing and genomic analysis were outsourced to Biotechnology Research Institute, Inc. (Sagamihara, Japan).

Sequencing libraries were prepared using the MGIEasy FS DNA Library Prep Set (MGI, Shenzhen, China) and the MGISP960 platform (MGI, Shenzhen, China), and sequencing was performed using a next-generation sequencer, a DNBSEQ-G400 platform (MGI, Shenzhen, China), generating 150 bp paired-end reads. Raw short-read sequences were obtained and processed using Trimmomatic v0.39 to remove adapter sequences and low-quality reads. Single-nucleotide variants (SNVs) and insertions/deletions (indels) were detected using Snippy v4.6.0 (https://github.com/tseemann/snippy, accessed on 25 November 2026). The processed reads were mapped to the EcudH parental reference genome (chromosome AP054613; plasmids AP054614 and AP054615). Large indels were identified by visual inspection of the read-mapping data using CLC Genomics Workbench (QIAGEN Digital Insights, Aarhus, Denmark) and Integrative Genomics Viewer (IGV; Broad Institute, Cambridge, MA, USA).

2.15. Determination of Minimum Inhibitory Concentrations (MICs)

MICs were determined by the broth microdilution method using Mueller–Hinton broth in 96-well microplates. Azithromycin, kanamycin, and amoxicillin were tested at final concentrations ranging from 0.06 to 128 μg mL^{-1} in twofold serial dilutions. The bacterial suspension was adjusted to a 0.5 McFarland standard and then diluted tenfold in Mueller–Hinton broth. A 5 μL aliquot of the diluted bacterial suspension was added to each well. The final bacterial concentration was adjusted to approximately 5×10^5 CFU/mL. The microplates were incubated at 37 °C for 24 h. The MIC was defined as the lowest

concentration of antimicrobial agent that completely inhibited visible bacterial growth compared with the growth control.

2.16. Time-Course Growth Analysis of Escherichia coli Strains in the Presence of Antibiotics

Clinical *E. coli* isolates or phage-resistant strains were grown to the logarithmic phase, and 200 μL of each bacterial suspension was dispensed into each well of a 96-well microtiter plate. Erythromycin or clarithromycin was added at final concentrations of 0, 2, 4, or 8 μg mL^{-1}. Bacterial growth was monitored by measuring OD_{600} every 15 min for 24 h at 37 °C with shaking using a microplate reader. Growth curves were generated based on changes in OD_{600} over time. Relative growth was calculated by dividing the OD_{600} at 24 h in the presence of antibiotics by that of the corresponding antibiotic-free culture of the same strain. Statistical analyses were performed using one-way analysis of variance (ANOVA) followed by Dunnett's multiple-comparison test, with each phage-resistant derivative compared with EcudH at the same antibiotic concentration. Significance levels are indicated as ** ($p < 0.01$) and **** ($p < 0.0001$).

2.17. Assessment of Bacterial Growth During Phage and Clarithromycin Treatment

EcudQ was grown to the logarithmic phase, and 200 μL of the bacterial suspension was dispensed into each well of a 96-well microplate. ΦH28-2 was added at a multiplicity of infection (MOI) of 0.1. A wider clarithromycin concentration series of 0, 1, 2, 4, 8, 16, and 32 μg mL^{-1} was examined. For the time-course analysis, clarithromycin was added at final concentrations of 0, 1, 2, or 4 μg mL^{-1}. Bacterial growth was monitored by measuring OD_{600} every 15 min for 24 h at 37 °C with shaking using a microplate reader. Growth curves were generated from OD_{600} measurements over time. OD_{600} values at 12 h were presented without normalization. Relative growth at 12 h was calculated by dividing the OD_{600} of each phage-treated culture by that of the corresponding untreated control at 12 h. Statistical analyses were performed using one-way analysis of variance (ANOVA) followed by Dunnett's multiple-comparison test, as indicated by the comparison brackets in the corresponding plots. Significance levels are indicated as ** ($p < 0.01$), *** ($p < 0.001$), and **** ($p < 0.0001$).

2.18. Use of Generative AI in Manuscript Preparation

Generative AI was used to assist with English-language editing, grammar checking, manuscript formatting, and refinement of the clarity and organization of the text, including the Discussion. All AI-assisted suggestions were reviewed and revised by the authors, who retained full responsibility for the scientific interpretations and conclusions.

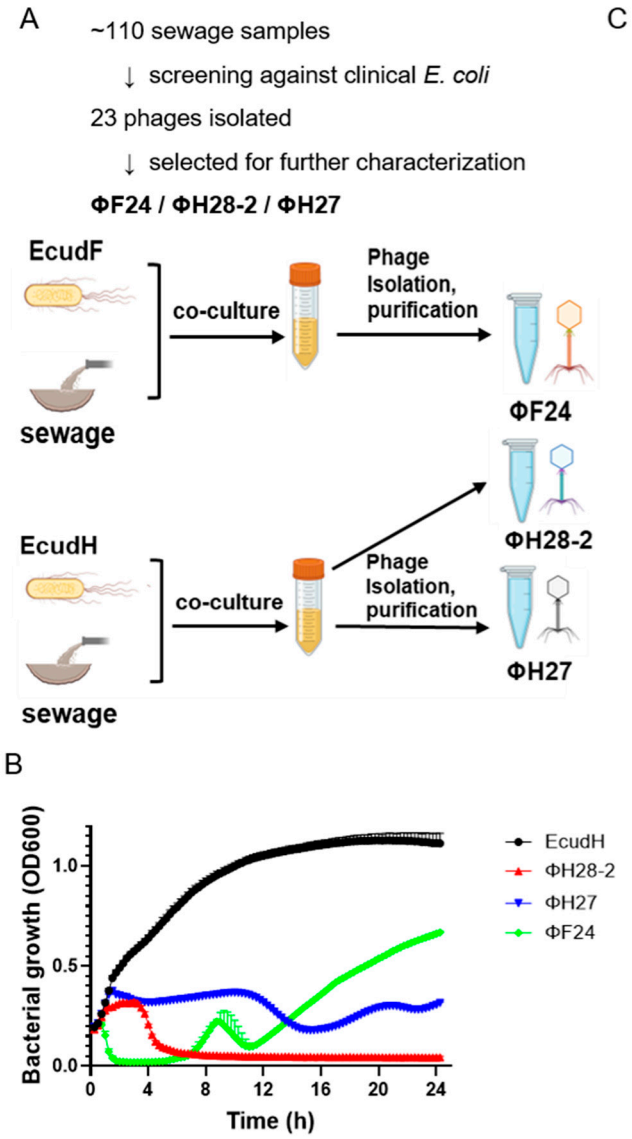
3. Results

3.1. Isolation, Lytic Activity, and Host Range of Phages Infecting Clinical E. coli Isolates

We screened approximately 110 sewage samples for phages active against a panel of 35 clinical *E. coli* isolates from companion animals with urinary tract infections. The screening yielded 23 phages. We selected ΦF24, ΦH28-2, and ΦH27 for further characterization based on reproducible plaque formation and lytic activity (Figure 1A). ΦF24 was isolated using EcudF as the host, whereas ΦH28-2 and ΦH27 were isolated using EcudH.

In microplate-reader assays with EcudH, ΦH28-2 suppressed bacterial growth over the 24 h observation period, with OD_{600} remaining low after approximately 5 h. ΦH27 reduced growth relative to the phage-free control, although OD_{600} fluctuated throughout the assay. ΦF24 caused rapid initial suppression, followed by a transient increase in OD_{600}

at approximately 8–9 h and sustained bacterial regrowth after approximately 12 h (Figure 1B).



C

Efficiency of plating (EOP)

	Φ		
	F24	H28-2	H27
ECud-A	1.05	-	-
ECud-B	-	-	-
ECud-C	0.17	0.21	-
ECud-D	-	-	-
ECud-E	0.29	0.08	-
ECud-F	0.62	0.69	-
ECud-G	-	-	-
ECud-H	1.00	1.00	1.00
ECud-I	-	-	-
ECud-J	-	-	-
ECud-K	1.22	-	0.26
ECud-L	-	-	-
ECud-M	0.91	0.49	-
ECud-N	1.03	-	-
ECud-O	1.08	-	0.37
ECud-P	-	-	-
ECud-Q	0.89	0.27	0.31
ECud-R	-	-	-
ECud-S	-	-	-
ECud-T	1.08	0.96	-
ECud-U	-	0.50	-
ECud-V	-	-	-
ECud-W	0.92	0.64	-
ECud-X	0.37	0.42	-
ECud-Y	0.22	0.09	-
ECud-Z	-	-	-
ECud-AA	-	-	-
ECud-AD	-	-	-
ECud-AE	0.32	0.43	-
ECud-AF	1.11	0.70	-
ECud-AG	-	-	-
ECud-AH	-	-	-
ECud-AI	0.32	0.38	-
ECud-AJ	-	-	-
ERIKA	0.18	0.22	-

Color intensity indicates EOP (darker green represents higher EOP).
–, no detectable plaque formation.

Figure 1. Isolation, lytic activity, and host range of ΦF24, ΦH28-2, and ΦH27. (**A**) Schematic of the phage isolation and selection workflow. Arrows indicate the sequence of the isolation and selection steps. Approximately 110 sewage samples were screened for phages using a panel of 35 clinical *E. coli* isolates, yielding 23 phages. ΦF24 was isolated using EcudF, whereas ΦH28-2 and ΦH27 were isolated using EcudH. (**B**) Growth kinetics of EcudH cultured without phage (control) or with ΦF24, ΦH28-2, or ΦH27. The bacterial suspension was adjusted to an OD_{600} of approximately 0.4, and 200 µL was dispensed into each well. For phage treatment, 20 µL of phage suspension (10^7 PFU/mL) was added. OD_{600} was monitored for 24 h using a microplate reader. Lines show mean OD_{600} values, and error bars indicate SD (three technical replicates). (**C**) Heatmap of the efficiency of plating (EOP) of the three phages across 35 clinical *E. coli* isolates. For each phage, EOP was calculated as the phage titer on each test isolate divided by the titer on EcudH. All 35 clinical isolates are shown. EOP values are shown for all isolates with detectable plaque formation; all of these isolates also showed growth inhibition in plate reader assays. Darker green indicates higher EOP, and a dash indicates no

detectable plaque formation under the assay conditions. Created in BioRender. Mana, T. (2026) (https://BioRender.com/ndyttdw, accessed on 25 November 2026)

EOP assays across the 35 clinical isolates showed that ΦF24 and ΦH28-2 formed plaques on 18 and 15 isolates, respectively, whereas ΦH27 formed plaques on only four isolates (Figure 1C). Thus, ΦF24 and ΦH28-2 had broader host ranges among these clinical isolates than ΦH27.

3.2. Phylogenetic and Comparative Genomic Analyses of ΦF24, ΦH28-2, and ΦH27

Whole-genome phylogenetic analyses placed ΦF24 and ΦH28-2 within the genus *Tequatrovirus* and ΦH27 within the genus *Felixounavirus* (Figure 2A,B). Transmission electron microscopy revealed isometric capsids and contractile tails in all three phages, consistent with a myovirus-like morphology (Figure S3). Genomic characteristics, including genome length, G+C content, predicted coding sequences, and tRNA genes, are summarized in Table 1.

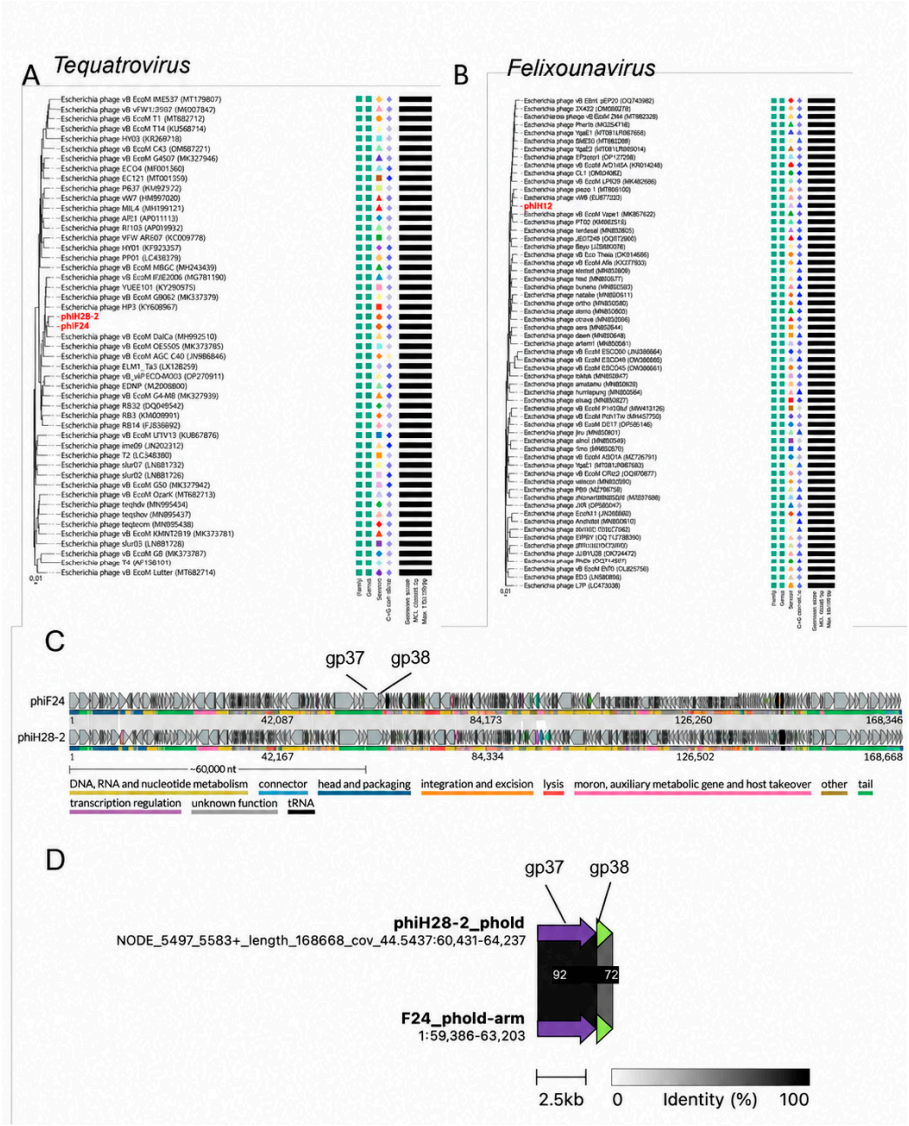


Figure 2. Whole-genome phylogenetic and comparative genomic analyses of ΦF24, ΦH28-2, and ΦH27. Whole-genome phylogenies were inferred from nucleotide sequences using the Genome BLAST Distance Phylogeny (GBDP) method implemented in VICTOR with distance formula D0. (**A**) Phylogenetic placement of ΦF24 and ΦH28-2 among phages assigned to the genus *Tequatrovirus*. (**B**) Phylogenetic placement of ΦH27 among phages assigned to the genus *Felixounavirus*. Different

shapes and colors indicate family-, genus-, and species-level taxonomic clusters suggested by VICTOR, as well as G+C content. Black horizontal bars represent genome lengths. The phages characterized in this study are highlighted in red. (**C**) Whole-genome comparison of ΦF24 and ΦH28-2 generated using LoVis4u. Predicted coding sequences are shown as arrows, and the colored bars beneath them indicate predicted functional categories. Gray links between the genomes indicate homologous regions. The positions of gp37 and gp38 are indicated. The displayed coordinates do not necessarily correspond to the full lengths of the genome sequences. (**D**) Expanded comparison of the region containing the tail-associated genes gp37 and gp38. The numbers within the connecting blocks indicate pairwise amino acid sequence identity between the corresponding proteins, as calculated using clinker (Gp37, 92%; Gp38, 72%). The grayscale represents amino acid sequence identity from 0% to 100%, with darker shading indicating higher identity. The scale bar represents 2.5 kb.

Table 1. Genomic characteristics of ΦF24, ΦH28-2, and ΦH27.

Phage	Genome Length (bp)	G+C (%)	Predicted CDSs	tRNA Genes	Genus	Accession Number
ΦF24	168,457	35%	295	10	*Tequatrovirus*	LC969012
ΦH28-2	168,668	35%	291	10	*Tequatrovirus*	LC969014
ΦH27	88,113	39%	151	24	*Felixounavirus*	LC969013

Whole-genome comparison of ΦF24 and ΦH28-2 revealed extensive synteny across most of their genomes (Figure 2C). The region containing the tail-associated genes *gp37* and *gp38* also retained conserved gene order; however, the predicted Gp37 and Gp38 protein sequences of the two phages shared 92% and 72% amino acid sequence identity, respectively, as determined using clinker (Figure 2D). The greater divergence of Gp38 relative to Gp37 suggests that variation in this tail-associated protein may be associated with differences in host recognition between ΦF24 and ΦH28-2, although its functional role was not experimentally examined in this study.

3.3. Resistance to ΦH27 and ΦH28-2 Is Associated with Mutations Affecting Distinct Steps in LPS Core Biosynthesis

To identify genetic changes associated with phage resistance, EcudH was separately co-cultured with ΦH27 or ΦH28-2 for 48 h. Surviving colonies were purified, and their phage susceptibility was reassessed. Two ΦH27-resistant derivatives, mtH27a and mtH27b, and two ΦH28-2-resistant derivatives, mtH28-2(1) and mtH28-2(2), were selected for further characterization (Figure 3A; Table 2).

Table 2. Resistance-associated variants in EcudH-derived phage-resistant strains.

Derivative	Selecting Phage	Gene	Nucleotide Variants	Predicted Effect	Function	Candidate Structure/Factor
mtH27a	ΦH27	*waaO*	T:300 TA:0	frameshift	LPS outer-core biosynthesis	LPS outer core
mtH27b	ΦH27	*waaT*	T:363 G:0; T:589 C:0	stop; synonymous	LPS outer-core biosynthesis	LPS outer core
mtH28-2(1)	ΦH28-2	*hldE*	—	frameshift	ADP-heptose/inner-core biosynthesis	LPS inner core
mtH28-2(2)	ΦH28-2	*waaC*	C:80 T:0; G:77 T:2; GT:81 AC:1	missense; other variants	LPS inner-core biosynthesis	LPS inner core
mtF24d	ΦF24	*ompA*	G:247 C:4	stop	Outer membrane protein	OmpA

mtF24e	ΦF24	*ompA*	GGCGTTCA:244 G:12	frameshift	Outer membrane protein	OmpA

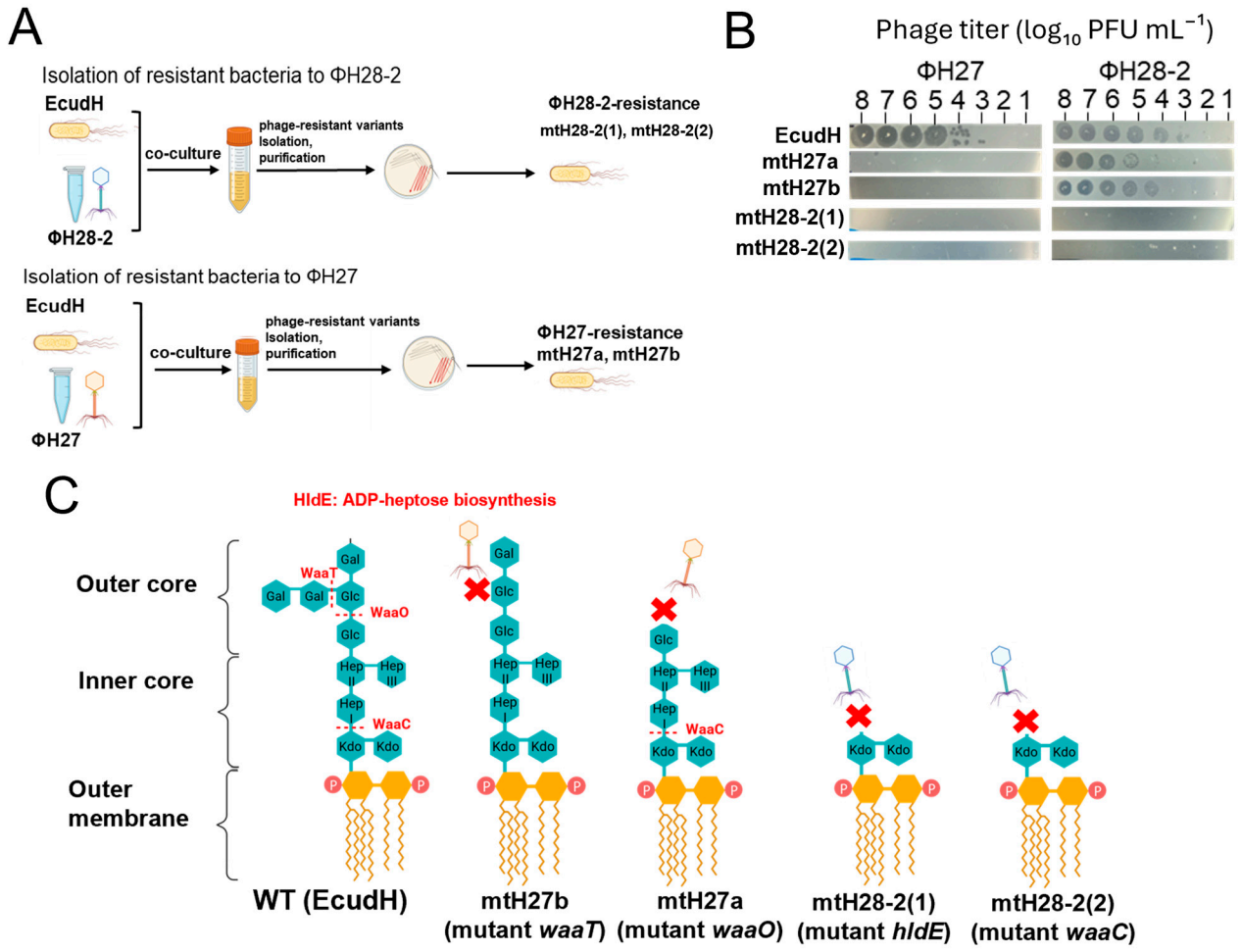


Figure 3. Isolation and characterization of ΦH27- and ΦH28-2-resistant *E. coli* derivatives. (**A**) Schematic workflow used to isolate phage-resistant derivatives. EcudH was separately co-cultured with ΦH27 or ΦH28-2 for 48 h, after which surviving colonies were isolated, purified, and retested for phage susceptibility. The selected derivatives were mtH27a and mtH27b from the ΦH27-exposed culture and mtH28-2(1) and mtH28-2(2) from the ΦH28-2-exposed culture. (**B**) Susceptibility of parental EcudH and the four resistant derivatives to ΦH27 and ΦH28-2, assessed by spot assay using tenfold serial phage dilutions ranging from 10^8 to 10^1 PFU/mL. Visible zones of lysis indicate phage susceptibility under the assay conditions. (**C**) Schematic representation of the predicted effects of the identified mutations on LPS core biosynthesis and structure. The predicted LPS structures of the parental strain EcudH and the phage-resistant derivatives mtH27b, mtH27a, and mtH28-2(2), carrying mutations in *waaT*, *waaO*, and *waaC*, respectively, are shown for comparison. The *hldE* mutation in mtH28-2(1) is illustrated separately as a potential disruption of HldE-dependent ADP-heptose biosynthesis. Red crosses indicate the predicted effects of the mutations on the respective biosynthetic steps, and phage symbols indicate the phage used to select each resistant derivative. The LPS structures and the effects of the mutations on LPS biosynthesis are inferred from the annotated functions of the affected genes and have not been experimentally confirmed. Dashed lines indicate the sites of action of the respective glycosyltransferases. Created in BioRender. Mana, T. (2026) (https://BioRender.com/ndyttdw, accessed on 25 November 2026)

Spot assays using tenfold serial phage dilutions showed that mtH27a and mtH27b were resistant to ΦH27 but remained susceptible to ΦH28-2. In contrast, mtH28-2(1) and mtH28-2(2) showed no detectable lysis by either ΦH27 or ΦH28-2 (Figure 3B).

Whole-genome sequencing identified candidate resistance-associated mutations in genes involved in LPS core biosynthesis (Table 2), and their predicted effects on LPS core structure are schematically illustrated in Figure 3C. mtH27a carried a deletion in *waaO* predicted to cause a frameshift, whereas mtH27b carried two single-nucleotide substitutions in *waaT*, one resulting in a premature stop codon and the other being synonymous. Both *waaO* and *waaT* are involved in LPS outer-core biosynthesis. mtH28-2(1) carried a deletion in *hldE* predicted to cause a frameshift, whereas mtH28-2(2) carried multiple nucleotide variants in *waaC*, including a missense substitution. *hldE* is required for ADP-heptose biosynthesis, whereas *waaC* encodes heptosyltransferase I, which catalyzes the addition of the first heptose residue to the LPS inner core.

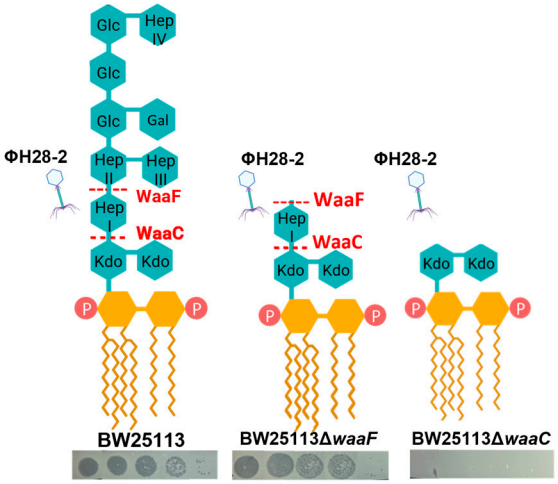
Together, the asymmetric cross-resistance pattern and the locations of the identified mutations support a model in which ΦH27 depends on specific outer-core features, whereas ΦH28-2 remains active against outer-core mutants but appears to require ADP-heptose-dependent inner-core assembly. By comparison, the ΦF24-resistant EcudH derivatives mtF24d and mtF24e carried a nonsense mutation and a frameshift-causing insertion in *ompA*, respectively (Table 2), implicating OmpA as a candidate host factor for ΦF24.

3.4. LPS Inner-Core Integrity Is Required for ΦH28-2 Infection and Influences Antibiotic Susceptibility and Bacterial Growth

To define the LPS structures required for ΦH28-2 infection, spot assays using tenfold serial phage dilutions were performed with *E. coli* BW25113 and its isogenic Δ*waaF* and Δ*waaC* mutants. ΦH28-2 produced detectable lysis on BW25113 and Δ*waaF* but not on Δ*waaC* (Figure 4A). WaaC catalyzes the addition of the first heptose residue (HepI) to the LPS inner core, whereas WaaF acts downstream by adding the second heptose residue (HepII). Thus, Δ*waaF* retains HepI, whereas Δ*waaC* lacks HepI and downstream core structures. These results identify a WaaC-dependent inner-core structure containing HepI as necessary for ΦH28-2 infection, although they do not establish HepI itself as the direct receptor.

To assess antibiotic susceptibility in strains carrying mutations in LPS core biosynthesis genes, MICs were measured for EcudH, mtH27a, mtH27b, mtH28-2(1), and mtH28-2(2).The azithromycin MICs were 16 μg mL^{-1} for EcudH, mtH27a and mtH27b, but decreased to 2 μg mL^{-1} for both mtH28-2(1) and mtH28-2(2). In contrast, the MICs of amoxicillin remained at 4 μg mL^{-1} in all tested strains, whereas the MIC of kanamycin was 2 μg mL^{-1} in mtH28-2(2) and 4 μg mL^{-1} in all other strains (Figure 4B). These results indicate that the reduced azithromycin MIC was associated with the ΦH28-2-resistant variants, whereas the MICs of amoxicillin and kanamycin showed little variation among the tested strains.

A



B

		MIC (μg mL⁻¹)				
Class	**Antibiotic**	**EcudH**	**mtH27a**	**mtH27b**	**mtH28-2(1)**	**mtH28-2(2)**
Hydrophobic	Azithromycin	16	16	16	2	2
Hydrophilic	Kanamycin	4	4	4	4	2
Hydrophilic	Amoxicillin	4	4	4	4	4

C

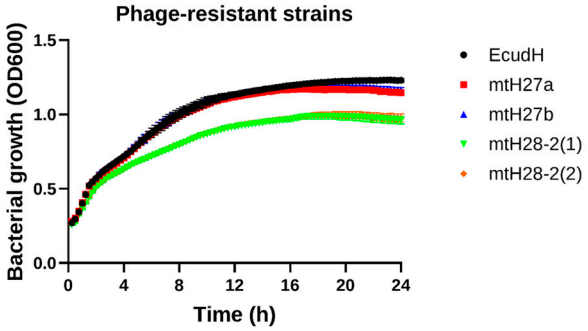
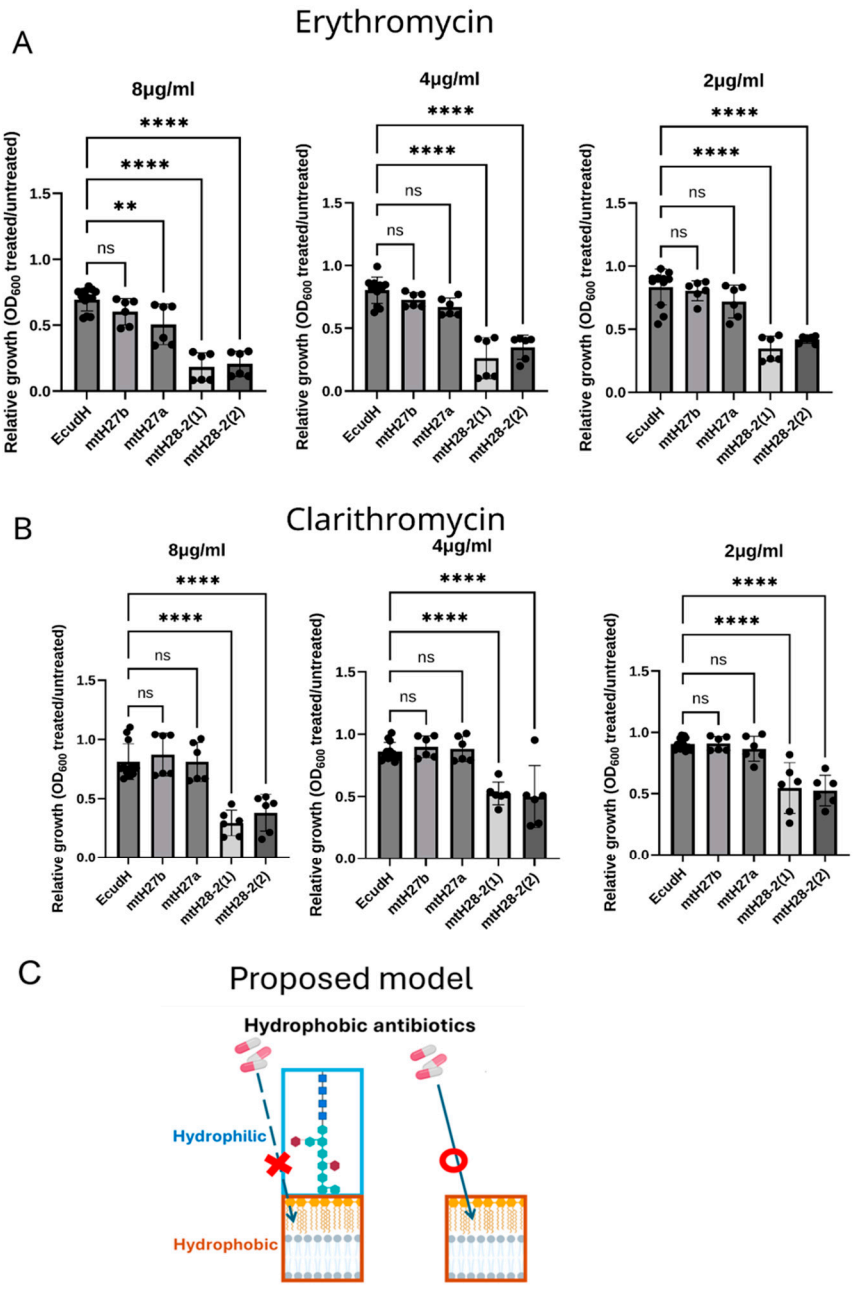


Figure 4. Requirement for a WaaC-dependent LPS inner-core structure for ΦH28-2 infection and effects of LPS alterations on antibiotic susceptibility and bacterial growth. (**A**) Susceptibility of *E. coli* BW25113 and its isogenic Δ*waaF* and Δ*waaC* mutants to ΦH28-2, assessed by spot assay using tenfold serial phage dilutions. The schematics show the predicted LPS structures of the parental and mutant strains. Δ*waaF* retains HepI but lacks HepII and downstream structures, whereas Δ*waaC* lacks HepI and subsequent core structures. Dashed lines indicate the sites of action of the respective glycosyltransferases. (**B**) MICs of the hydrophobic antibiotic azithromycin and the hydrophilic antibiotics kanamycin and amoxicillin for EcudH, mtH27a, mtH27b, mtH28-2(1) and mtH28-2(2). MIC values are expressed in μg mL^{-1}. (**C**) Growth kinetics of EcudH, mtH27a, mtH27b, mtH28-2(1), and mtH28-2(2) in antibiotic-free medium. Bacterial growth was monitored as OD_{600} for 24 h using a microplate reader. Lines and error bars indicate the mean and SD, respectively, from three technical replicates (n = 3). Created in BioRender. Mana, T. (2026) (https://BioRender.com/ndyttdw, accessed on 25 November 2026)

Growth kinetics were examined in antibiotic-free medium to distinguish baseline growth differences from antibiotic-dependent effects. The ΦH27-resistant derivatives mtH27a and mtH27b displayed growth profiles broadly similar to those of EcudH. In contrast, the *hldE* mutant mtH28-2(1) and *waaC* mutant mtH28-2(2) maintained a lower OD_{600} throughout most of the incubation period and reached a lower final OD_{600} at 24 h (Figure 4C; Table 2). These findings indicate that mtH28-2(1) and mtH28-2(2) exhibited reduced growth yield under antibiotic-free conditions.

3.5. Phage-Resistant Derivatives with LPS Core Mutations Show Increased Growth Inhibition by Macrolides

Because an intact LPS layer contributes to the outer-membrane permeability barrier against hydrophobic antibiotics, we examined the effects of erythromycin and clarithromycin on EcudH and four phage-resistant derivatives carrying mutations in LPS core biosynthesis genes. For each strain, OD_{600} at 24 h in the presence of antibiotic was normalized to that in the corresponding antibiotic-free culture (Figure 5A,B).



https://doi.org/10.3390/v18121344

Figure 5. Growth inhibition of phage-resistant *E. coli* derivatives carrying LPS core biosynthesis mutations by erythromycin and clarithromycin. Relative growth of EcudH, mtH27a, mtH27b, mtH28-2(1), and mtH28-2(2) during exposure to (**A**) erythromycin or (**B**) clarithromycin at 2, 4, or 8 μg mL^{-1}. Relative growth was calculated for each strain as OD_{600} at 24 h in the presence of the antibiotic divided by OD_{600} at 24 h in the corresponding antibiotic-free culture. Bars and error bars represent the mean and SD, respectively. Individual points represent measurements from three technical replicates in each independent experiment. At each antibiotic concentration, each phage-resistant derivative was compared with the parental strain EcudH using one-way ANOVA followed by Dunnett's multiple-comparison test. Brackets indicate the corresponding comparisons. ns, not significant; **, $p < 0.01$; ****, $p < 0.0001$. (**C**) Proposed model in which LPS core truncation may compromise the outer-membrane permeability barrier and facilitate access of hydrophobic macrolides. Membrane permeability was not directly measured. Red circles and crosses indicate facilitated and restricted antibiotic penetration, respectively. Arrows indicate the proposed direction of antibiotic penetration. Blue and orange boxes represent the hydrophilic and hydrophobic regions, respectively. Created in BioRender. Mana, T. (2026) (https://BioRender.com/ndyttdw, accessed on 25 November 2026)

At 2, 4, and 8 μg mL^{-1}, the ΦH28-2-resistant derivatives mtH28-2(1) and mtH28-2(2), carrying mutations in *hldE* and *waaC*, respectively, showed the lowest relative growth during exposure to either erythromycin or clarithromycin. The ΦH28-2-resistant derivatives exhibited greater macrolide-associated growth inhibition than the ΦH27-resistant derivatives, although the magnitude of the effect varied depending on antibiotic concentration.

Together with the azithromycin MIC results, these findings indicate that phage-selected alterations in LPS core biosynthesis are associated with increased susceptibility to hydrophobic macrolides. We propose that truncation of the hydrophilic LPS core weakens the outer-membrane permeability barrier and thereby facilitates access of hydrophobic macrolides to the bacterial cell (Figure 5C).

3.6. Clarithromycin Further Suppresses Bacterial Growth During ΦH28-2 Treatment

To assess bacterial growth during combined phage and macrolide exposure, EcudQ was treated with ΦH28-2 at a multiplicity of infection of 0.1 together with clarithromycin. Unnormalized OD_{600} values at 12 h were compared across a broader clarithromycin concentration range of 0–32 μg mL^{-1} (Figure 6A). In the focused concentration range of 0–4 μg mL^{-1}, bacterial growth was monitored for 24 h (Figure 6B), and relative growth at 12 h, normalized to the corresponding untreated EcudQ control, was compared between the phage-only and phage–clarithromycin groups (Figure 6C). Under the conditions tested, addition of clarithromycin reduced growth compared with phage alone at 12 h (Figure 6A,C). However, because a clarithromycin-only group was not included, the effects of the combination relative to clarithromycin alone and the presence of pharmacological synergy could not be determined.

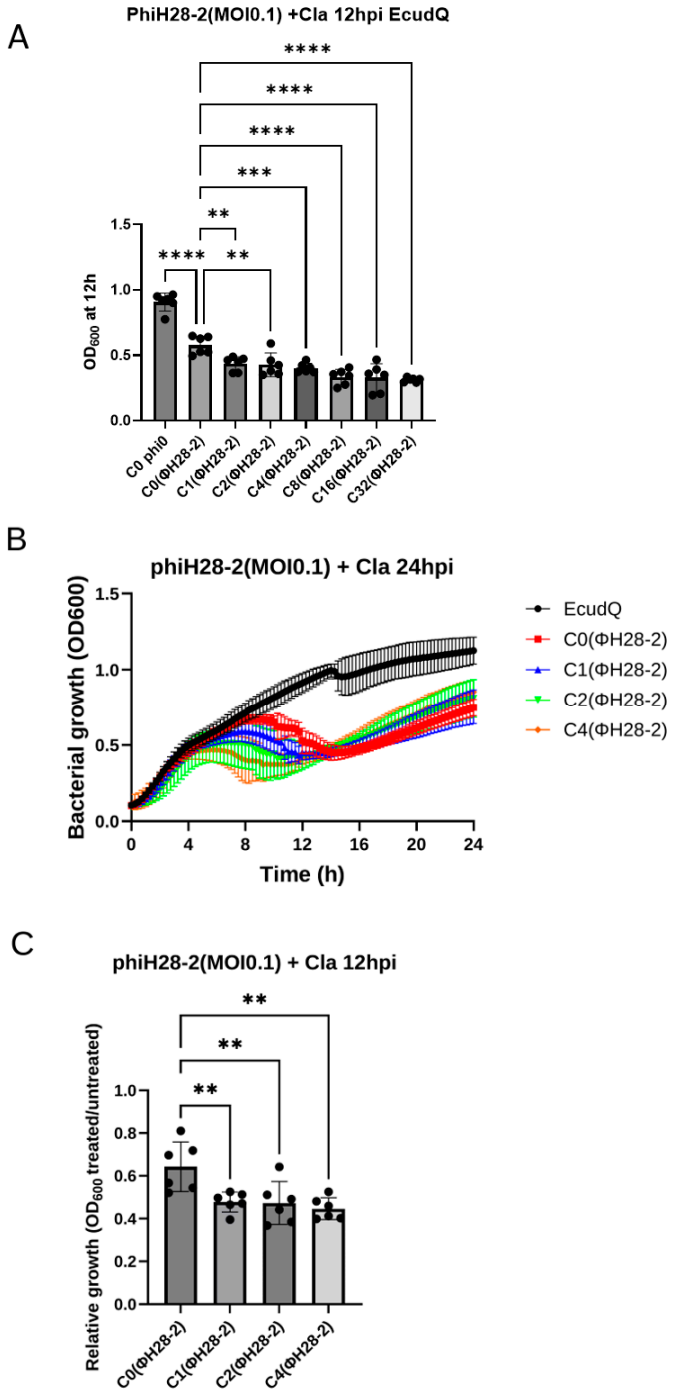


Figure 6. Effects of clarithromycin concentration on bacterial growth during ΦH28-2 treatment. EcudQ was exposed to ΦH28-2 at a multiplicity of infection of 0.1 with clarithromycin at the indicated concentrations. (**A**) Unnormalized OD_{600} values at 12 h in an expanded clarithromycin concentration series (0–32 μg mL^{-1}), including the untreated EcudQ and phage-only controls. (**B**) Growth kinetics measured as OD_{600} for 24 h in untreated EcudQ, ΦH28-2 alone, or ΦH28-2 together with 1, 2, or 4 μg mL^{-1} clarithromycin. (**C**) Relative growth at 12 h in the lower-concentration series (0–4 μg mL^{-1}), calculated relative to the untreated EcudQ control. The phage-only group contained ΦH28-2 and no clarithromycin. Bars and error bars indicate the mean and standard deviation (SD), respectively, with individual measurements shown as points. The statistical comparisons are indicated by brackets; **, $p < 0.01$; ***, $p < 0.001$; ****, $p < 0.0001$.

https://doi.org/10.3390/v18121344

4. Discussion

Host-range estimates can differ between spot tests and EOP assays [40]. Our results further illustrate the value of assessing bacterial growth dynamics alongside plaque formation when selecting therapeutic candidates. In particular, sustained growth suppression by ΦH28-2 in vitro is encouraging, but does not imply that resistance is unlikely, as resistant derivatives emerged upon longer exposure. The isolation host may also shape the diversity of recovered phages. The O-antigen type of EcudH could not be assigned by in silico serotyping, raising the possibility, but not demonstrating, a rough LPS phenotype. If its O-antigen is absent or reduced, otherwise shielded LPS core structures might be more accessible during phage isolation [41]. Conversely, O-antigen-deficient hosts may fail to recover phages that depend on O-antigen for infection [42]. Direct LPS profiling and comparisons between matched rough and smooth isolation hosts would be required to test this possibility.

Although ΦF24 and ΦH28-2 are genetically related T4-like phages [43,44], their differing activity profiles suggest that conserved genome organization does not ensure identical host recognition. Variation in tail-associated proteins, particularly Gp38, is a plausible contributor because such structures can influence adsorption and host specificity [45,46]. This explanation remains a hypothesis based on sequence comparison; neither the binding specificity nor the functional contribution of Gp37 or Gp38 was directly assessed here.

The occurrence of *ompA* variants in ΦF24-resistant EcudH derivatives nominates OmpA as a candidate host factor rather than establishing it as the receptor. OmpA has roles in envelope physiology and pathogenicity [47] and has been implicated in infection by other *E. coli* phages [46]. Its conservation could help explain ΦF24 activity across multiple isolates, although alternative routes to resistance cannot be excluded. If the resistance-associated variants impair OmpA function, additional phenotypic effects might arise, consistent with the roles of OmpA in postinvasion pathogenicity [48] and envelope stability and stress tolerance [49]. Complementation and direct binding experiments would be needed to distinguish receptor usage from indirect effects of envelope remodeling.

The contrasting resistance patterns of ΦH27 and ΦH28-2 suggest that distinct portions of the LPS core contribute to susceptibility. The Keio mutant findings support a requirement for a WaaC-dependent inner-core architecture containing heptose I during ΦH28-2 infection, but do not identify heptose I as the direct binding epitope. A relatively conserved inner core could support activity against multiple isolates, yet *E. coli* core types and modifications vary [50], while O-antigen shielding [41] and intracellular defenses such as restriction–modification systems [42] may still limit productive infection. Beyond phage susceptibility, core-biosynthesis defects can influence envelope integrity, surface properties, and response to antimicrobial agents [51,52]. The lower growth yield of the ΦH28-2-resistant derivatives in antibiotic-free broth is compatible with a growth-associated cost under the conditions tested. This interpretation is consistent with the reduced growth in human urine and impaired bladder colonization reported for phage-resistant uropathogenic *E. coli* by Zulk et al. [17], but our findings do not demonstrate reduced virulence or urinary-tract fitness.

The increase in macrolide-associated growth inhibition and reduction in azithromycin MIC among ΦH28-2-resistant derivatives identify a potentially useful trade-off accompanying phage escape. O-antigen chain length can also influence outer-membrane barrier function, with longer O-antigen chains increasing susceptibility to selected antibiotics in experimental *E. coli* and *Shigella flexneri* models [53]. Defects in LPS-core biosynthesis can alter outer-membrane properties and increase susceptibility to hydrophobic antibiotics, including macrolides [9,51,52]. In *E. coli*, limited outer-

membrane penetration and active efflux normally constrain macrolide activity [8,9]. Accordingly, our observations are consistent with increased outer-membrane permeability in the resistant derivatives; however, drug uptake and permeability were not measured, and other physiological consequences of the LPS mutations may contribute. Because O-antigen expression in EcudH was not directly assessed, the relative contributions of inner-core alterations and any accompanying changes in O-antigen display also remain unresolved.

The combination experiment provides preliminary support for evaluating ΦH28-2 alongside clarithromycin, because co-exposure produced greater growth suppression at 12 h than phage treatment alone under the conditions tested. Nevertheless, this assay used EcudQ rather than the LPS-mutant EcudH derivatives, so it does not demonstrate that the additional suppression results from the resistance-associated changes described above. Furthermore, the absence of a clarithromycin-only control and a formal interaction analysis precludes any claim of pharmacological synergy. Previous studies have explored phage–antibiotic combinations to enhance bacterial suppression or control regrowth [54,55], but their effects depend on the phage, antibiotic, strain, and exposure conditions. Testing matched bacterial backgrounds, antibiotic-only controls, and urine-relevant conditions is therefore essential before interpreting these observations as a therapeutic benefit.

The potential relevance of these findings to human UTIs extends beyond the animal origin of the isolates. Genomic studies have identified *E. coli* lineages associated with UTIs in both humans and companion animals, although the overall population structures differ and transmission between hosts was not examined in this study [56]. Human clinical investigations are also evaluating phage-based approaches for *E. coli* UTIs, including early-phase assessment of phage-cocktail pharmacokinetics, tolerability, and bacteriological responses [57]. Our findings support investigating whether phage selection strategies that account for both antibacterial activity and resistance-associated trade-offs could inform future veterinary and human therapeutic development. However, the phages described here have not been tested against human UTI isolates, and the macrolide susceptibility shifts observed in vitro do not establish clinical efficacy. Erythromycin and clarithromycin are not standard first-line treatments for uncomplicated *E. coli* UTIs; clinically relevant urinary drug exposure and treatment outcomes must therefore be evaluated before proposing their therapeutic use. More broadly, steering phage resistance toward bacterial vulnerabilities merits further study [58,59].

This study has several limitations. All antibacterial activities and resistance-associated phenotypes were measured under in vitro conditions, so their relevance to the urinary tract environment remains uncertain. Although ΦH28-2-resistant derivatives exhibited lower OD_{600} in antibiotic-free broth, competitive fitness, virulence, and bladder colonization were not directly assessed. In addition, the urinary pharmacokinetics and achievable concentrations of the tested macrolides, as well as the stability and lytic activity of ΦH28-2 in urine, require evaluation. Genetic and knockout experiments point to a WaaC-dependent inner-core structure, but direct adsorption, receptor-binding, complementation, and LPS structural analyses are needed to establish the mechanistic basis of susceptibility. Finally, the potential influence of O-antigen shielding on host range remains untested in matched rough and smooth bacterial backgrounds.

5. Conclusions

This study identified and characterized bacteriophages targeting *E. coli* from companion-animal UTIs and showed that resistance to ΦH28-2 can coincide with alterations in LPS inner-core biosynthesis, reduced bacterial growth yield, and increased macrolide susceptibility in vitro. These observations support considering resistance-

associated phenotypic trade-offs alongside host range and lytic activity during phage selection. Although the contribution of individual LPS structures to adsorption and the clinical relevance of the antibiotic phenotype remain unresolved, this approach may guide future investigations of phage–antibiotic strategies in veterinary medicine and, potentially, human urinary tract infections.

Supplementary Materials: The following supporting information can be downloaded at: https://www.mdpi.com/article/10.3390/v18121344/s1, Figure S1, core-genome phylogenetic relationships among clinical *Escherichia coli* isolates; Figure S2, host-range screening of 23 bacteriophages against 35 clinical *Escherichia coli* isolates; Figure S3, transmission electron micrographs of ΦH27, ΦH28-2, and ΦF24; Table S1, characteristics of the *E. coli* strains used in this study.

Author Contributions: Conceptualization, H.I. (Hidetomo Iwano) and J.F. (including the hypothesis regarding changes in antibiotic susceptibility associated with phage resistance); methodology and investigation (phage isolation and characterization), M.T. and H.O.; formal analysis (genomic analysis), T.N. and K.M.; investigation (minimum inhibitory concentration assays), N.I., M.E. and H.I. (Hiroki Inoue); investigation (transmission electron microscopy), T.I.; writing—original draft preparation, M.T. and H.I. (Hidetomo Iwano); writing—review and editing, M.T. and H.I. (Hidetomo Iwano); supervision and project administration, H.I. (Hidetomo Iwano). All authors have read and agreed to the published version of the manuscript.

Funding: This research was funded by the Japan Agency for Medical Research and Development (AMED), grant JP25gm1610002 (H.I.), and JSPS KAKENHI, grants JP23K23791 (J.F.) and JP23KJ2059 (T.N.). This study was also supported in part by collaborative research funding provided by NDTS Co., Ltd. to Rakuno Gakuen University, including support for laboratory consumables shared among phage research projects. This study was also supported by the Japan Agency for Medical Research and Development (AMED) through the Translational Research Program at Hokkaido University (Seed A, A562; Grant Numbers JP25ym0126801 and JP26ym0126801). The article processing charge was supported by the same program in fiscal year 2026.

Institutional Review Board Statement: Not applicable. This study used bacterial isolates obtained during routine veterinary diagnostic procedures and did not involve experimental procedures on live animals.

Informed Consent Statement: Not applicable.

Data Availability Statement: The assembled phage genome sequences were assigned DDBJ accession numbers LC969012 (ΦF24), LC969014 (ΦH28-2), and LC969013 (ΦH27). The complete EcudH genome is registered under AP054613 (chromosome), AP054614 (plasmid 1), and AP054615 (plasmid 2), associated with BioProject PRJDB45974 and BioSample SAMD02121473. Genomic typing information for the other clinical *Escherichia coli* isolates is provided in Supplementary Table S1. Additional data supporting the findings are available from the corresponding author upon reasonable request.

Acknowledgments: During the preparation of this manuscript, the authors used ChatGPT (GPT-6.2; OpenAI, San Francisco, CA, USA) for English-language editing, grammar checking, manuscript formatting, and refinement of the clarity and organization of the text. The authors independently assessed the scientific content, reviewed and edited AI-assisted suggestions, and take full responsibility for the published content.

Conflicts of Interest: Rakuno Gakuen University has a collaborative research agreement with NDTS Co., Ltd. and receives research funding from the company. Hidetomo Iwano is involved in this collaboration. Naomi Iwano, Masashi Ebisawa, and Hiroki Inoue are employees of NDTS Co., Ltd. These relationships have been disclosed to and reviewed by the Conflict of Interest Committee of

Rakuno Gakuen University, which determined that the collaboration was acceptable under the university's institutional policies. The authors declare no other conflicts of interest.

References

1. Antimicrobial Resistance Collaborators. Global burden of bacterial antimicrobial resistance in 2019: A systematic analysis. *Lancet* **2022**, *399*, 629–655. https://doi.org/10.1016/S0140-6736(21)02724-0.
2. Sati, H.; Carrara, E.; Savoldi, A.; Hansen, P.; Garlasco, J.; Campagnaro, E.; Boccia, S.; Castillo-Polo, J.A.; Magrini, E.; Garcia-Vello, P.; et al. The WHO Bacterial Priority Pathogens List 2024: A prioritisation study to guide research, development, and public health strategies against antimicrobial resistance. *Lancet Infect. Dis.* **2025**, *25*, 1033–1043. https://doi.org/10.1016/S1473-3099(25)00118-5.
3. Poolman, J.T.; Wacker, M. Extraintestinal Pathogenic *Escherichia coli*, a Common Human Pathogen: Challenges for Vaccine Development and Progress in the Field. *J. Infect. Dis.* **2016**, *213*, 6–13.
4. Flores-Mireles, A.L.; Walker, J.N.; Caparon, M.; Hultgren, S.J. Urinary tract infections: Epidemiology, mechanisms of infection and treatment options. *Nat. Rev. Microbiol.* **2015**, *13*, 269–284.
5. Laupland, K.B.; Ross, T.; Pitout, J.D.D.; Church, D.L.; Gregson, D.B. Community-onset urinary tract infections: A population-based assessment. *Infection* **2007**, *35*, 150–153.
6. Carmona-Cartaya, Y.; Hidalgo-Benito, M.; Borges-Mateus, L.M.; Pereda-Novales, N.; González-Molina, M.K.; Quiñones-Pérez, D. Community-Acquired Uropathogenic *Escherichia coli*, Antimicrobial Susceptibility, and Extended-Spectrum Beta-Lactamase Detection. *MEDICC Rev.* **2022**, *24*, 20–25.
7. Marques, C.; Gama, L.T.; Belas, A.; Bergström, K.; Beurlet, S.; Briend-Marchal, A.; Broens, E.M.; Costa, M.; Criel, D.; Damborg, P.; et al. European multicenter study on antimicrobial resistance in bacteria isolated from companion animal urinary tract infections. *BMC Vet. Res.* **2016**, *12*, 213. https://doi.org/10.1186/s12917-016-0840-3.
8. Myers, A.G.; Clark, R.B. Discovery of Macrolide Antibiotics Effective against Multi-Drug Resistant Gram-Negative Pathogens. *Acc. Chem. Res.* **2021**, *54*, 1635–1645.
9. Vaara, M. Outer membrane permeability barrier to azithromycin, clarithromycin, and roxithromycin in gram-negative enteric bacteria. Antimicrob. *Agents Chemother.* **1993**, *37*, 354–356.
10. Nikaido, H. Molecular basis of bacterial outer membrane permeability revisited. Microbiol. *Mol. Biol. Rev.* **2003**, *67*, 593–656.
11. Fujiki, J.; Nakamura, K.; Nakamura, T.; Iwano, H. Fitness Trade-Offs between Phage and Antibiotic Sensitivity in Phage-Resistant Variants: Molecular Action and Insights into Clinical Applications for Phage Therapy. *Int. J. Mol. Sci.* **2023**, *24*, 15628. https://doi.org/10.3390/ijms242115628.
12. Nakamura, K.; Fujiki, J.; Nakamura, T.; Furusawa, T.; Gondaira, S.; Usui, M.; Higuchi, H.; Tamura, Y.; Iwano, H. Fluctuating Bacteriophage-induced galU Deficiency Region is Involved in Trade-off Effects on the Phage and Fluoroquinolone Sensitivity in Pseudomonas aeruginosa. *Virus Res.* **2021**, *306*, 198596. https://doi.org/10.1016/j.virusres.2021.198596.
13. Gordillo Altamirano, F.; Forsyth, J.H.; Patwa, R.; Kostoulias, X.; Trim, M.; Subedi, D.; Archer, S.K.; Morris, F.C.; Oliveira, C.; Kielty, L.; et al. Bacteriophage-resistant Acinetobacter baumannii are resensitized to antimicrobials. *Nat. Microbiol.* **2021**, *6*, 157–161. https://doi.org/10.1038/s41564-020-00830-7.
14. Freitag, T.; Squires, R.A.; Schmid, J. Naturally occurring bacteriophages lyse a large proportion of canine and feline uropathogenic *Escherichia coli* isolates in vitro. *Res. Vet. Sci.* **2008**, *85*, 1–7.
15. Burmeister, A.R.; Fortier, A.; Roush, C.; Lessing, A.J.; Bender, R.G.; Barahman, R.; Grant, R.; Chan, B.K.; Turner, P.E. Pleiotropy complicates a trade-off between phage resistance and antibiotic resistance. *Proc. Natl. Acad. Sci. USA* **2020**, *117*, 11207–11216. https://doi.org/10.1073/pnas.1919888117.
16. McGee, L.W.; Barhoush, Y.; Shima, R.; Hennessy, M. Phage-resistant mutations impact bacteria susceptibility to future phage infections and antibiotic response. *Ecol. Evol.* **2023**, *13*, e9712.
17. Zulk, J.J.; Clark, J.R.; Ottinger, S.; Ballard, M.B.; Mejia, M.E.; Mercado-Evans, V.; Heckmann, E.R.; Sanchez, B.C.; Trautner, B.W.; Maresso, A.W.; et al. Phage Resistance Accompanies Reduced Fitness of Uropathogenic *Escherichia coli* in the Urinary Environment. *mSphere* **2022**, *7*, e0034522. https://doi.org/10.1128/msphere.00345-22.
18. Baba, T.; Ara, T.; Hasegawa, M.; Takai, Y.; Okumura, Y.; Baba, M.; Datsenko, K.A.; Tomita, M.; Wanner, B.L.; Mori, H. Construction of *Escherichia coli* K-12 in-frame, single-gene knockout mutants: The Keio collection. *Mol. Syst. Biol.* **2006**, *2*, 2006.0008. https://doi.org/10.1038/msb4100050.

19. Furusawa, T.; Iwano, H.; Higuchi, H.; Yokota, H.; Usui, M.; Iwasaki, T.; Tamura, Y. Bacteriophage can lyse antibiotic-resistant Pseudomonas aeruginosa isolated from canine diseases. *J. Vet. Med. Sci.* **2016**, *78*, 1035–1038. https://doi.org/10.1292/jvms.15-0310.
20. Fujiki, J.; Furusawa, T.; Munby, M.; Kawaguchi, C.; Matsuda, Y.; Shiokura, Y.; Nakamura, K.; Nakamura, T.; Sasaki, M.; Usui, M.; et al. Susceptibility of Pseudomonas aeruginosa veterinary isolates to Pbunavirus PB1-like phages. *Microbiol. Immunol.* **2020**, *64*, 778–782. https://doi.org/10.1111/1348-0421.12846.
21. Bonilla, N.; Rojas, M.I.; Netto Flores Cruz, G.; Hung, S.H.; Rohwer, F.; Barr, J.J. Phage on tap-a quick and efficient protocol for the preparation of bacteriophage laboratory stocks. *PeerJ* **2016**, *4*, e2261.
22. Bolger, A.M.; Lohse, M.; Usadel, B. Trimmomatic: A flexible trimmer for Illumina sequence data. *Bioinformatics* **2014**, *30*, 2114–2120.
23. Wick, R.R.; Judd, L.M.; Gorrie, C.L.; Holt, K.E. Unicycler: Resolving bacterial genome assemblies from short and long sequencing reads. *PLoS Comput. Biol.* **2017**, *13*, e1005595.
24. Martin, M. Cutadapt removes adapter sequences from high-throughput sequencing reads. *EMBnet.journal* **2011**, *17*, 10–12. https://doi.org/10.14806/ej.17.1.200.
25. Shen, W.; Le, S.; Li, Y.; Hu, F. SeqKit: A Cross-Platform and Ultrafast Toolkit for FASTA/Q File Manipulation. *PLoS ONE* **2016**, *11*, e0163962.
26. Wick, R.R. Porechop: Adapter Trimmer for Oxford Nanopore Reads (Version 0.2.3). Available online: https://github.com/rrwick/Porechop (accessed on 30 October 2026).
27. Wick, R.R.; Schultz, M.B.; Zobel, J.; Holt, K.E. Bandage: Interactive visualization of de novo genome assemblies. *Bioinformatics* **2015**, *31*, 3350–3352.
28. Parks, D.H.; Imelfort, M.; Skennerton, C.T.; Hugenholtz, P.; Tyson, G.W. CheckM: Assessing the quality of microbial genomes recovered from isolates, single cells, and metagenomes. *Genome Res.* **2015**, *25*, 1043–1055.
29. Bouras, G.; Nepal, R.; Houtak, G.; Psaltis, A.J.; Wormald, P.J.; Vreugde, S. Pharokka: A fast scalable bacteriophage annotation tool. *Bioinformatics* **2023**, *39*, btac776. https://doi.org/10.1093/bioinformatics/btac776.
30. Bouras, G.; Grigson, S.R.; Mirdita, M.; Heinzinger, M.; Papudeshi, B.; Mallawaarachchi, V.; Green, R.; Kim, R.S.; Mihalia, V.; Psaltis, A.J.; et al. Protein structure-informed bacteriophage genome annotation with Phold. *Nucleic Acids Res.* **2026**, *54*, gkaf1448. https://doi.org/10.1093/nar/gkaf1448.
31. Egorov, A.A.; Atkinson, G.C. LoVis4u: A locus visualization tool for comparative genomics and coverage profiles. *NAR Genom. Bioinform.* **2025**, *7*, lqaf009.
32. Gilchrist, C.L.M.; Chooi, Y.H. clinker & clustermap.js: Automatic generation of gene cluster comparison figures. *Bioinformatics* **2021**, *37*, 2473–2475.
33. Meier-Kolthoff, J.P.; Göker, M. VICTOR: Genome-based phylogeny and classification of prokaryotic viruses. *Bioinformatics* **2017**, *33*, 3396–3404.
34. Seemann, T. Prokka: Rapid prokaryotic genome annotation. *Bioinformatics* **2014**, *30*, 2068–2069.
35. Jolley, K.A.; Bray, J.E.; Maiden, M.C.J. Open-access bacterial population genomics: BIGSdb software, the PubMLST.org website and their applications. *Wellcome Open Res.* **2018**, *3*, 124.
36. Bessonov, K.; Laing, C.; Robertson, J.; Yong, I.; Ziebell, K.; Gannon, V.P.J.; Nichani, A.; Arya, G.; Nash, J.H.E.; Christianson, S. ECTyper: In silico *Escherichia coli* serotype and species prediction from raw and assembled whole-genome sequence data. *Microb. Genom.* **2021**, *7*, 000728. https://doi.org/10.1099/mgen.0.000728.
37. Tonkin-Hill, G.; MacAlasdair, N.; Ruis, C.; Weimann, A.; Horesh, G.; Lees, J.A.; Gladstone, R.A.; Lo, S.; Beaudoin, C.; Floto, R.A.; et al. Producing polished prokaryotic pangenomes with the Panaroo pipeline. *Genome Biol.* **2020**, *21*, 180. https://doi.org/10.1186/s13059-020-02090-4.
38. Wong, T.K.F.; Ly-Trong, N.; Ren, H.; Demotte, P.; Baños, H.; Roger, A.J.; Susko, E.; Bielow, C.; De Maio, N.; Goldman, N.; et al. IQ-TREE 3: Phylogenomic inference software using complex evolutionary models. *Mol. Biol. Evol.* **2026**, *43*, msag117. https://doi.org/10.1093/molbev/msag117.
39. Letunic, I.; Bork, P. Interactive Tree of Life (iTOL) v6: Recent updates to the phylogenetic tree display and annotation tool. *Nucleic Acids Res.* **2024**, *52*, W78–W82.
40. Khan Mirzaei, M.; Nilsson, A.S. Isolation of phages for phage therapy: A comparison of spot tests and efficiency of plating analyses for determination of host range and efficacy. *PLoS ONE* **2015**, *10*, e0118557.
41. Letarov, A.V. Bacterial Virus Forcing of Bacterial O-Antigen Shields: Lessons from Coliphages. *Int. J. Mol. Sci.* **2023**, *24*, 17390. https://doi.org/10.3390/ijms242417390.

42. Humolli, D.; Piel, D.; Maffei, E.; Heyer, Y.; Agustoni, E.; Shaidullina, A.; Willi, L.; Imwinkelried, P.; Estermann, F.; Cuénod, A.; et al. Completing the BASEL phage collection to unlock hidden diversity for systematic exploration of phage-host interactions. *PLoS Biol.* **2025**, *23*, e3003063. https://doi.org/10.1371/journal.pbio.3003063.
43. Lavigne, R.; Darius, P.; Summer, E.J.; Seto, D.; Mahadevan, P.; Nilsson, A.S.; Ackermann, H.W.; Kropinski, A.M. Classification of Myoviridae bacteriophages using protein sequence similarity. *BMC Microbiol.* **2009**, *9*, 224. https://doi.org/10.1186/1471-2180-9-224.
44. Petrov, V.M.; Ratnayaka, S.; Nolan, J.M.; Miller, E.S.; Karam, J.D. Genomes of the T4-related bacteriophages as windows on microbial genome evolution. *Virol. J.* **2010**, *7*, 292.
45. Nobrega, F.L.; Vlot, M.; de Jonge, P.A.; Dreesens, L.L.; Beaumont, H.J.E.; Lavigne, R.; Dutilh, B.E.; Brouns, S.J.J. Targeting mechanisms of tailed bacteriophages. *Nat. Rev. Microbiol.* **2018**, *16*, 760–773. https://doi.org/10.1038/s41579-018-0070-8.
46. Lutz, V.T.; Klein-Sousa, V.; Bojer, M.S.; Van Overfelt, S.S.F.; Nugen, S.R.; Taylor, N.M.I.; Gambino, M.; Brøndsted, L. Gp38 adhesins of Straboviridae phages recognize specific extracellular loops of outer membrane protein receptors. *npj Viruses* **2025**, *3*, 37. https://doi.org/10.1038/s44298-025-00118-9.
47. Confer, A.W.; Ayalew, S. The OmpA family of proteins: Roles in bacterial pathogenesis and immunity. *Vet. Microbiol.* **2013**, *163*, 207–222.
48. Nicholson, T.F.; Watts, K.M.; Hunstad, D.A. OmpA of uropathogenic *Escherichia coli* promotes postinvasion pathogenesis of cystitis. *Infect. Immun.* **2009**, *77*, 5245–5251.
49. Wang, Y. The function of OmpA in *Escherichia coli.* Biochem. Biophys. *Res. Commun.* **2002**, *292*, 396–401.
50. Amor, K.; Heinrichs, D.E.; Frirdich, E.; Ziebell, K.; Johnson, R.P.; Whitfield, C. Distribution of core oligosaccharide types in lipopolysaccharides from *Escherichia coli*. *Infect. Immun.* **2000**, *68*, 1116–1124.
51. Wang, J.; Ma, W.; Fang, Y.; Liang, H.; Yang, H.; Wang, Y.; Dong, X.; Zhan, Y.; Wang, X. Core Oligosaccharide Portion of Lipopolysaccharide Plays Important Roles in Multiple Antibiotic Resistance in *Escherichia coli*. Antimicrob. *Agents Chemother.* **2021**, *65*, e0034121. https://doi.org/10.1128/AAC.00341-21.
52. Pagnout, C.; Sohm, B.; Razafitianamaharavo, A.; Caillet, C.; Offroy, M.; Leduc, M.; Gendre, H.; Jomini, S.; Beaussart, A.; Bauda, P.; et al. Pleiotropic effects of rfa-gene mutations on *Escherichia coli* envelope properties. *Sci. Rep.* **2019**, *9*, 9696. https://doi.org/10.1038/s41598-019-46100-3
53. May, K.L.; Akiyama, T.; Parker, B.G.; Kim, M.; Grabowicz, M. LPS O-antigen polysaccharide length impacts outer membrane permeability of enteric gram-negative bacteria. *mBio* **2025**, *16*, e0251825.
54. Gu Liu, C.; Green, S.I.; Min, L.; Clark, J.R.; Salazar, K.C.; Terwilliger, A.L.; Kaplan, H.B.; Trautner, B.W.; Ramig, R.F.; Maresso, A.W. Phage-Antibiotic Synergy Is Driven by a Unique Combination of Antibacterial Mechanism of Action and Stoichiometry. *mBio* **2020**, *11*, e01462-20. https://doi.org/10.1128/mBio.01462-20.
55. Makky, S.; Hussein, A.H.; Mohamed, A.A.; Essam, K.; Agwa, M.M.; Abd ElAziz, M.M.; El-Shibiny, A. Can phage-antibiotic combinations overcome uropathogenic *Escherichia coli* regrowth? evidence from in vitro and in vivo models. *Virol. J.* **2026**, *23*, 50. https://doi.org/10.1186/s12985-026-03067-8.
56. Jousserand, N.; Auvray, F.; Chagneau, C.; Cavalié, L.; Maurey, C.; Drut, A.; Lavoué, R.; Oswald, E. Zoonotic potential of uropathogenic *Escherichia coli* lineages from companion animals. *Vet. Res.* **2025**, *56*, 69. https://doi.org/10.1186/s13567-025-01493-0.
57. Kim, P.; Sanchez, A.M.; Penke, T.J.R.; Tuson, H.H.; Kime, J.C.; McKee, R.W.; Slone, W.L.; Conley, N.R.; McMillan, L.J.; Prybol, C.J.; et al. Safety, pharmacokinetics, and pharmacodynamics of LBP-EC01, a CRISPR-Cas3-enhanced bacteriophage cocktail, in uncomplicated urinary tract infections due to *Escherichia coli* (ELIMINATE): The randomised, open-label, first part of a two-part phase 2 trial. *Lancet Infect. Dis.* **2024**, *24*, 1319–1332. https://doi.org/10.1016/S1473-3099(24)00424-9.
58. Gurney, J.; Pradier, L.; Griffin, J.S.; Gougat-Barbera, C.; Chan, B.K.; Turner, P.E.; Kaltz, O.; Hochberg, M.E. Phage steering of antibiotic-resistance evolution in the bacterial pathogen, Pseudomonas aeruginosa. *Evol. Med. Public Health* **2020**, *2020*, 148–157. https://doi.org/10.1093/emph/eoaa026.
59. Cardoso, L.L.; Gaissmaier, M.S.; von Strempel, A.; Keys, T.; Matchado, M.S.; Salvado Silva, M.; Ring, D.; Slack, E.; Stecher, B. In vitro and in vivo selection and cost of bacteriophage resistance on natural *Escherichia coli*. *microLife* **2025**, *6*, uqaf017. https://doi.org/10.1093/femsml/uqaf017.

Disclaimer/Publisher's Note: The statements, opinions and data contained in all publications are solely those of the individual author(s) and contributor(s) and not of MDPI and/or the editor(s). MDPI and/or the editor(s) disclaim responsibility for any injury to people or property resulting from any ideas, methods, instructions or products referred to in the content.